

Chiral and Critical Spin Liquids in Spin-1/2 Kagome Antiferromagnet

W. Zhu, S. S. Gong, and D. N. Sheng

Department of Physics and Astronomy, California State University, Northridge, California 91330, USA

The topological quantum spin liquids (SL) and the nature of quantum phase transitions between them have attracted intensive attentions for the past twenty years. The extended kagome spin-1/2 antiferromagnet emerges as the primary candidate for hosting both time reversal symmetry (TRS) preserving and TRS breaking SLs based on density matrix renormalization group simulations. To uncover the nature of the novel quantum phase transition between the SL states, we study a minimum XY model with the nearest neighbor (NN) (J_{xy}), the second and third NN couplings ($J_{2xy} = J_{3xy} = J'_{xy}$). We identify the TRS broken chiral SL (CSL) with the turn on of a small perturbation $J'_{xy} \sim 0.06J_{xy}$, which is fully characterized by the fractionally quantized topological Chern number and the conformal edge spectrum as the $\nu = 1/2$ fractional quantum Hall state. On the other hand, the NN XY model ($J'_{xy} = 0$) is shown to be a critical SL state adjacent to the CSL, characterized by the gapless spin singlet excitations and also vanishing small spin triplet excitations. The quantum phase transition from the CSL to the gapless critical SL is driven by the collapsing of the neutral (spin singlet) excitation gap. By following the evolution of entanglement spectrum, we find that the transition takes place through the coupling of the edge states with opposite chiralities, which merge into the bulk and become gapless neutral excitations. The effect of the NN spin- z coupling J_z is also studied, which leads to a quantum phase diagram with an extended regime for the gapless SL.

PACS numbers: 73.43.Nq, 75.10.Jm, 75.10.Kt

Quantum spin liquid (SL) is an exotic state of matter which escapes from forming the conventional orders even at zero temperature [1]. However, different from a featureless insulator, a SL develops a topological order [2–4] with fractionized quasiparticles encoded in the long-range entanglement of system [5]. The SL physics may play a fundamental role for understanding strongly correlated systems and unconventional superconductivity [6–21]. There have been intensive studies searching for SL in frustrated magnetic systems, however, the discovery of SL has been rare in the past 20 years. A few frustrated square or honeycomb lattices spin systems with competing interactions have been proposed as the candidates for gapped SL [22–25]. However, further studies find that the competing plaquette valence-bond solid may dominate the magnetic disorder region [26–29].

Interestingly, the nearest neighbor (NN) dominant spin-1/2 kagome Heisenberg model has been identified to host a gapped SL based on the state of art density matrix renormalization group (DMRG) calculations [30–33], where a near quantized topological entanglement entropy [34, 35] has been found consistent with a Z_2 SL [32, 33]. The topological degeneracy as a signature evidence for such a gapped topological state [2, 8–10, 36] has not been established, while different methods have been applied to tackle this problem [31, 37]. Meanwhile, the variational studies find that the Dirac gapless SL has the lower variational energy among different states based on the projected fermionic parton wavefunctions [38, 39]. The nature of the SL in the kagome Heisenberg model remains not fully understood.

By introducing the second- and third- NN couplings for the spin-1/2 kagome systems, DMRG studies [40, 41] discover the Kalmeyer-Laughlin CSL theoretically predicted more than 20 years ago [42–46], which spontaneously breaks TRS and is identified as the $\nu = 1/2$ fractional quantum Hall (FQH) state [42, 43, 47]. Interestingly, the CSL state is also found in

the spin anisotropic kagome model involving the second and third NN xy -plane couplings [48], or by introducing the TRS breaking three-spin chiralities interactions [49]. However, the nature of the quantum phase transition, especially how the quantum state and entanglement spectrum (ES) evolve near such a transition have not been addressed. We do not know what a physical mechanism can drive the quantum phase transition in such a system, and if the emergence of the previously identified gapped SL for the NN kagome Heisenberg model has close connection with the collapsing of the CSL [50]. Our work is motivated to address these open questions.

Along with theoretical developments, experiments also discover different promising SL candidates in the triangular organic compounds [51–53] and kagome antiferromagnets Herbertsmithite and Kapellasite $\text{Cu}_3\text{Zn}(\text{OH})_6\text{Cl}_2$ in recent years [54–59]. These materials appear to have gapless excitations as revealed by the specific heat and neutron scattering measurements [55–58]. Thus, it would be extremely interesting to also search for some minimum spin-1/2 kagome model which can host a gapless SL.

In this Letter, we address the nature of the collapsing of CSL and the related phase transition in kagome spin system based on DMRG and exact diagonalization (ED) calculations. We study the spin-1/2 XXZ kagome model with the spin XY interactions for the second and third neighbors as shown in the inset of Fig. 1(a), whose Hamiltonian is given as [48]

$$H = (J_{xy}/2) \sum_{\langle i,j \rangle} (S_i^+ S_j^- + h.c.) + J_z \sum_{\langle i,j \rangle} S_i^z S_j^z + (J'_{xy}/2) \sum_{\langle i,j \rangle'} (S_i^+ S_j^- + h.c.), \quad (1)$$

where the summations are taken over the NN $\langle i,j \rangle$, the second and third NN $\langle i,j \rangle'$ couplings. We set $J_{xy} = 1$ as energy scale. Our main results are summarized as the phase diagram

in Fig. 1(a). First of all, for the XY model with $J_z = 0$, we establish a CSL for $J'_{xy} \gtrsim 0.06$ based on the topological features of the state: the conformal chiral edge spectrum in accordance with the $\nu = 1/2$ FQH state and the topological quantized Chern number $C = 1/2$. We identify the physical driving force for the destruction of the CSL as the collapsing of the singlet excitation gap with reducing J'_{xy} . Following the evolution of ES, we find that the phase transition takes place through the coupling between the low-lying entanglement states with opposite chiralities, which naturally leads to a critical state with TRS and gapless neutral excitations [60, 61]. Our results represent a significant progress in understanding the connection between different SLs [48] by identifying the mechanism of the phase transition and establishing the characteristic nature of the critical SL phase adjacent to the CSL. After tuning on the NN spin- z coupling J_z , we identify the phase diagram for different J'_{xy} , where the critical gapless SL is found for an extended regime with small $J'_{xy} \sim 0$. The connection of the critical SL with the previously identified gapped SL in Heisenberg model [31] will also be discussed.

We use DMRG [62] and ED to study cylinder and torus systems with the geometry shown in the inset of Fig. 1(a). The number of sites in cylinder (open boundary condition in the x -direction) or torus system is $N = 3 \times L_y \times L_x$ with L_x and L_y as the numbers of unit cell in the x and y directions [63]. We perform the flux insertion simulations on cylinder systems based on the newly developed adiabatic DMRG to detect the topological Chern number [40]. In this simulation, we thread a flux θ in the cylinder which is equivalent to imposing the twist boundary conditions: $S_i^+ S_j^- + h.c. \rightarrow e^{i\theta_{ij}} S_i^+ S_j^- + h.c.$ for these bonds crossing the y boundary. In DMRG studies we keep up to 8000 – 10000 states for the simulations without flux and 4500 – 6000 states in the flux insertion simulations for accurate results.

Chiral spin liquid phase.— The CSL breaks TRS but preserves lattice symmetries and spin rotational symmetry. The TRS broken is usually detected by the chiral order parameter $\chi_i = (S_{i_1} \times S_{i_2}) \cdot S_{i_3}$ ($i_1, i_2, i_3 \in \Delta_i(\nabla_i)$ triangle) [44]. As shown in Fig. 1(b), we demonstrate the chiral correlations $\langle \chi_i \chi_j \rangle$ between the up-triangles i and j as a function of distance R_{ij} for the XY model ($J_z = 0$). At $J'_{xy} = 0$, the chiral correlations decay exponentially to vanish. With growing J'_{xy} , the chiral correlations enhance gradually and appear to approach finite values for $J'_{xy} \gtrsim 0.2$ at large distance, which indicates the emerging long-range chiral order that characterizes the spontaneous TRS breaking.

Moreover, CSL is a topological ordered state that hosts two-fold topological degenerate groundstates, which can be obtained by inserting flux with $\theta = 0 \rightarrow 2\pi$ adiabatically [40]. The ES for these two states, labeled by the quantum number total S^z of the half system, and their relative momentum quantum number along the y direction Δk_y [64, 65], are shown in Figs. 1(c) and 1(d). The leading ES has the robust degeneracy pattern $\{1, 1, 2, 3, 5, 7, \dots\}$ with increasing Δk_y in each S^z sector, which follows the chiral $SU(2)_1$ Wess-Zumino-Witten conformal field theory description of the $\nu = 1/2$ FQH state

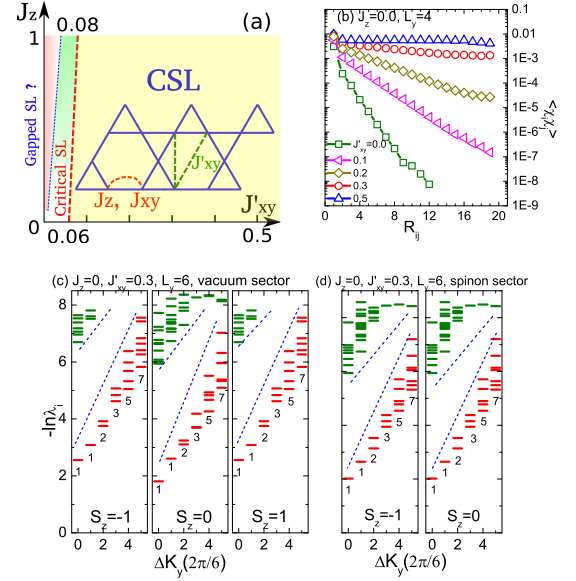


FIG. 1: (color online) (a) Schematic phase diagram of the spin-1/2 kagome model with Hamiltonian Eq. (1) for $0.0 \leq J'_{xy} \leq 0.5$, $0.0 \leq J_z \leq 1.0$, where both the CSL and a critical SL with gapless singlet excitations are identified. The color gradient in the critical SL denotes the growing spin gap on finite-size system with increasing J_z . The gapped SL [31] may exist neighboring with the critical SL. (b) Log-linear plot of chiral correlation $\langle \chi_i \chi_j \rangle$ versus the distance of triangles R_{ij} along the x direction in the vacuum sector (c) and (d) are the ES of the groundstates in the vacuum and spinon sectors, respectively. λ_i is the eigenvalue of reduced density matrix. The numbers $\{1, 1, 2, 3, 5, 7, \dots\}$ label the near degenerating pattern for the low-lying ES with different relative momentum Δk_y and total spin S^z .

[66] as the fingerprint for the emergence of the CSL [67]. The spectra of the vacuum ($\theta = 0$) and spinon ($\theta = 2\pi$) sectors are symmetric about $S^z = 0$ and $-\frac{1}{2}$ respectively, indicating a spin- $\frac{1}{2}$ spinon at each end of cylinder in the spinon sector.

Fractional quantization of topological Chern number.— To reveal the full topological nature of the CSL phase, we perform the flux insertion simulation to obtain the topological Chern number [40]. By adiabatically inserting flux θ , we study the evolution of the spin- z magnetization $\langle S^z_{x,y} \rangle$ at each site $R_i = (x, y)$. One example with a small $\theta = \pi/4$ is shown in Fig. 2(a). We find that the nonzero magnetizations start to build up at both edges of cylinder after inserting flux. The net magnetization near boundaries grows monotonically with increasing θ as shown in Fig. 2(b), which is equivalent to the spin transfer being pumped from the left edge to the right edge without accumulating in the bulk. As shown in Fig. 2(c), a spin pump linearly increases with θ on $L_y = 6$ cylinder, which leads to a quantized net spin transfer $\Delta S^z|_{\text{edge}} = 0.500$ at $\theta = 2\pi$ and a quantized Chern number $C = 1/2$, fully characterizing the state as the $\nu = 1/2$ FQH state [40, 46, 68]. For the system with $L_y = 4$ as shown in the inset of Fig. 2(c), we find some finite size effect as the spin pump initially is zero for small θ , which jumps to the expected values of the

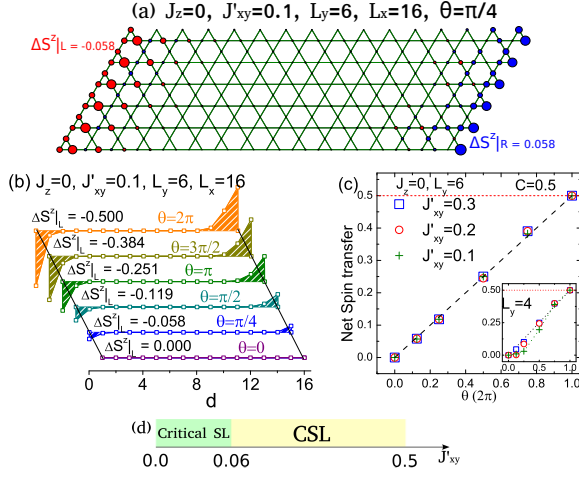


FIG. 2: (color online) (a) Spin magnetization $\langle S^z_{x,y} \rangle$ at $R_i = (x, y)$ after adiabatically inserting a flux $\theta = \pi/4$. The area of the circle is proportional to the amplitude of $\langle S^z_{x,y} \rangle$. The blue (red) color represents the positive (negative) $\langle S^z_{x,y} \rangle$. (b) Accumulated spin magnetization $\langle S^z_x \rangle = \sum_y \langle S^z_{x,y} \rangle$ in each column (the summation is over all the $3L_y$ sites for each column) with increasing flux θ . (c) Net spin transfer $\Delta S^z|_{\text{edge}}$ as a function of θ on $L_y = 6$ cylinder. The inset shows the results on $L_y = 4$ cylinder. (d) Phase diagram of the XY kagome model ($J_z = 0$), which is determined from the results of Chern number on $L_y = 6$ system.

linear pumping behavior at a larger θ for $J'_{xy} = 0.1, 0.2$. The CSL is protected by the finite bulk excitation gap (shown later in Fig. 4) and grows stronger with increasing system width. Based on the quantized Chern number established on $L_y = 6$ cylinder with different geometries [63] and the conformal edge spectrum for the groundstates, we find a robust CSL phase for $J'_{xy} \gtrsim 0.06$ as shown in the phase diagram Fig. 2(d) for $J_z = 0$. In the critical SL region, we observe strong magnetization fluctuations in the bulk during the process of inserting flux in consistent with the collapsing of the neutral excitation gap.

Entanglement spectrum flow.— The CSL and the critical state can be understood based on the response of ES to inserted flux [69, 70]. For a CSL at $J'_{xy} = 0.1$, as shown in Fig. 3(a), the eigenvalues of the reduced density matrix are degenerating about the $\pm S^z$ sectors at $\theta = 0$. By increasing θ , the spectrum lines in the positive S^z sectors flow up continuously, while those in the negative S^z sectors flow down (this is selected by the sign of Chern number due to spontaneous TRS breaking). At $\theta = 2\pi$, the eigenvalues in the $S^z = 0$ and $S^z = -1$ sectors become degenerate. As a result, after inserting a flux quantum, a net spin transfer $\Delta S|_L = \langle S^z|_L \rangle = \sum_i \lambda_i S^z_i = -1/2$ is realized and the spectrum becomes symmetric about $S^z = -1/2$. Thus the ES flow directly detects the gapless feature in the edge spectrum through inserting flux. By inserting 4π flux, the ES continues to flow and, it becomes symmetric about $S^z = -1$ at $\theta = 4\pi$, indicating two spinons have been transferred from the left edge to the right edge while the bulk of the system goes

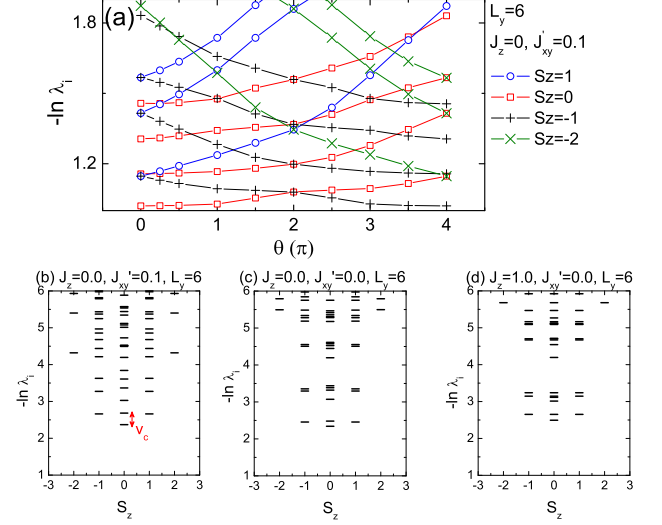


FIG. 3: (color online) (a) ES flow with inserting flux θ for $J_z = 0, J'_{xy} = 0.1$ on $L_y = 6$ cylinder. ES for (b) $J_z = 0.0, J'_{xy} = 0.1$, (c) $J_z = 0.0, J'_{xy} = 0.0$, and (d) $J_z = 1.0, J'_{xy} = 0.0$ on $L_y = 6$ cylinder. The arrow denoted by v_c in (b) indicates the two lowest eigenvalues in the $S^z = 0$ sector which are used to calculate the chiral edge-mode velocity.

back to the vacuum sector.

With decreasing J'_{xy} , the robust Chern number quantization and the spectrum flow persist to $J'_{xy} \simeq 0.06$. By following the evolution of the ES, we find that the CSL is becoming less strong at smaller J'_{xy} , where the chiral velocity (proportional to the gap between the lowest two spectrum levels in the $S^z = 0$ sector as indicated in Fig. 3(b)) [63] diminishes with decreasing J'_{xy} . As illustrated in Figs. 3(b) and 3(c), we observe that the ES as a function of quantum number S^z before and after the phase transition appear to be similar at $J'_{xy} = 0.1$ and 0.0 . However, they are significantly different in momentum space. The spectrum for $J'_{xy} = 0.1$ preserves the same robust conformal chiral edge spectrum as demonstrated in Fig. 1(c) with many entanglement eigenstates carrying nonzero k_y [63]. However, once the phase transition takes place, the groundstate wavefunction has TRS, and the low-lying entanglement states shown in Fig. 3(c) have the momentum quantum number k_y either 0 or π if they are nondegenerate, which comes from the mixing between eigenstates with opposite chiralities. Furthermore, these low-lying eigenstates do not respond to the inserted flux. The mixing of entanglement states with opposite chiralities illustrates what happens to the physical edge states [71]. These edge states with opposite chiralities also mix and merge into the bulk and become the low energy gapless excitations in the bulk. These observations are consistent with the field theory description for the quantum phase transition between two states with different Chern numbers [60, 61]. Interestingly, the ES for the NN kagome Heisenberg model in Fig. 3(d) is similar to the one of the NN XY model.

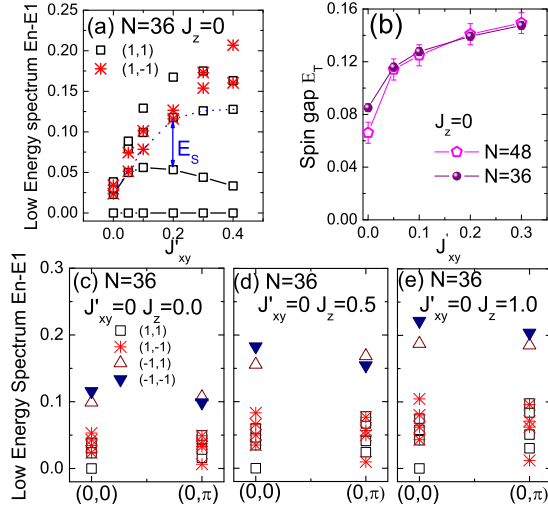


FIG. 4: (color online) (a) Evolution of the ED low-energy spectrum in the $k = (0,0)$ sector with J'_{xy} for the XY model ($J_z = 0$) on the $N = 3 \times 3 \times 4$ torus. The singlet gap between the lowest two groundstates and higher-energy states is denoted as E_s . (b) J'_{xy} dependence of spin gap E_T for the XY model on the $N = 3 \times 3 \times 4$ and $3 \times 4 \times 4$ tori. Low-energy spectrum of the NN XXZ model ($J'_{xy} = 0$) at $k = (0,0)$ and $(0,\pi)$ sectors for (c) $J_z = 0.0$, (d) $J_z = 0.5$, and (e) $J_z = 1.0$ on the $3 \times 3 \times 4$ torus. The label $(\pm 1, \pm 1)$ denote the quantum numbers related to spin inversion and lattice π -rotation symmetries.

Low-energy excitations.— We first study the evolution of the low-energy singlet excitations in the $S^z = 0$ sector as a function of J'_{xy} for the XY model ($J_z = 0$). As shown in Fig. 4(a) of the spectrum for 36-site torus system in $k = (0,0)$ sector, we find two low-energy near degenerate groundstates separated by a finite singlet gap E_s from higher energy excitations in the CSL phase at larger $J'_{xy} \simeq 0.3$ side [40]. With decreasing J'_{xy} , the singlet gap E_s reduces, which collapses to vanishing small at $J'_{xy} \sim 0 - 0.05$. Thus the quantum phase transition from the CSL to the TRS preserving state is driven by such a neutral excitation gap closing. For comparison, we also obtain the triplet gap E_T in DMRG calculations using torus systems with $N = 3 \times 4 \times 3$ and $3 \times 4 \times 4$ as shown in Fig. 4(b) [72]. Similarly, E_T drops with reducing J'_{xy} and it becomes much smaller for $N = 48$ system at $J'_{xy} = 0$. Thus, our results indicate that the critical state is centered near $J'_{xy} = 0$, where the singlet gap vanishes and the spin gap is very tiny or vanished (E_T reduces with N and $E_T \simeq 0.049$ for $N = 3 \times 5 \times 6$). The appearance of low-energy singlet excitations below the finite-size spin gap can be understood as the gapless neutral mode for the topological quantum phase transition [60, 61], which necessarily exists for such a transition.

We further study the whole phase diagram with varying J_z and J'_{xy} , where similar CSL to critical phase transition is observed as illustrated in the phase diagram Fig. 1(a). Furthermore, we examine the low energy spectra of the NN XXZ model ($J'_{xy} = 0$) on $N = 3 \times 4 \times 3$ torus system. As shown

in Figs. 4(c)-4(e) for $J_z = 0.0, 0.5$ and 1.0 , we find near continuous low energy excitations [73] collapsing together below the spin triplet gap, which implies the gapless singlet excitations in the whole critical SL region. The structure of the energy spectra remains very similar, which indicates that the spin interaction J_z term may only enhance the energy scale of excitations. The gapped SL [31] may exist neighboring with the critical SL close to the NN Heisenberg model and we cannot determine the precise phase boundary of the critical SL due to the limited system width we can access in DMRG simulations.

Summary and discussions.— We identify a TRS broken CSL phase with a small perturbation $J'_{xy} \simeq 0.06$ in the $J_{xy} - J'_{xy}$ XY model, while the NN XY model is in a critical phase adjacent to the CSL with vanishing singlet excitations and a small or vanishing spin triplet gap based on ED and DMRG studies. Furthermore, by studying the evolution of ES crossing the quantum phase transition, we identify that the quantum phase transition takes place through the coupling and mixing of the chiral states with opposite chiralities, which naturally lead to a critical state with TRS and gapless neutral excitations. The quantum phase transition appears to be very smooth, which is driven by the continuous closing of the gap for spin singlet excitations. However, it is important to mention that limited by the range of systems one can access using DMRG, one cannot determine if there is a discontinuity in the singlet gap at the transition point in thermodynamic limit. Thus the quantum phase transition can be a weakly first order or continuous transition, which demands study based on effective theory for these novel SL states. Finally, we find that the NN J_z coupling leads to a phase diagram with an extended regime for the critical SL possibly including or close to the NN Heisenberg kagome model. While the neutral excitation has to be gapless in such a critical SL, we find that the spin gap is possibly finite, but very small, which grows bigger with the increase of J_z . Our DMRG calculations for spin gap on larger tori and ED calculations for singlet gap indicate that these gaps decrease towards the NN models with reducing J'_{xy} , which are more consistent with a critical SL. However, the gapped Z_2 SL [31] may develop on larger systems in the NN models through opening the vison gap from the gapless neutral excitations outside the critical SL. This open and challenging question is desired to be addressed in the future based on different numerical methods and effective field theory approaches.

We hope to thank L. Balents, F. D. M. Haldane, L. Fu, P. A. Lee, T. Senthil, Z. Y. Weng, and especially X. G. Wen for stimulating discussions. We also thank Y. C. He and L. Cincio for their insightful discussions about developing infinite DMRG algorithm. This research is supported by the U.S. Department of Energy, Office of Basic Energy Sciences under grant No. DE-FG02-06ER46305 (W.Z., D.N.S.), the National Science Foundation through grants DMR-1408560 (S.S.G.).

-
- [1] L. Balents, *Nature* **464**, 199 (2010).
- [2] X. G. Wen, *Phys. Rev. B* **40**, 7387 (1989).
- [3] X. G. Wen and Q. Niu, *Phys. Rev. B* **41**, 9377 (1990).
- [4] X. G. Wen, *Int. J. Mod. Phys. B* **4**, 239 (1990).
- [5] X. Chen, Z. C. Gu, and X. G. Wen, *Phys. Rev. B* **82**, 155138 (2010).
- [6] P. W. Anderson, *Science* **235**, 1196 (1987).
- [7] D. S. Rokhsar and S. A. Kivelson, *Phys. Rev. Lett.* **61**, 2376 (1988).
- [8] N. Read and S. Sachdev, *Phys. Rev. Lett.* **66**, 1773 (1991).
- [9] X. G. Wen, *Phys. Rev. B* **44**, 2664 (1991).
- [10] T. Senthil and M.P.A. Fisher, *Phys. Rev. B* **62**, 7850 (2000); *Phys. Rev. Lett.* **86**, 292 (2001).
- [11] R. Moessner and S. L. Sondhi, *Phys. Rev. Lett.* **86**, 1881 (2001).
- [12] L. Balents, M. P. A. Fisher, and S. M. Girvin, *Phys. Rev. B* **65**, 224412 (2002).
- [13] T. Senthil and O. I. Motrunich, *Phys. Rev. B* **66**, 205104 (2002).
- [14] O. I. Motrunich and T. Senthil, *Phys. Rev. Lett.* **89**, 277004 (2002).
- [15] D. N. Sheng and L. Balents, *Phys. Rev. Lett.* **94**, 146805 (2005).
- [16] P. A. Lee, N. Nagaosa, and X. G. Wen, *Rev. Mod. Phys.* **78**, 17 (2006).
- [17] A. Kitaev, *Ann. Phys. (N.Y.)* **321**, 2 (2006).
- [18] D. F. Schroeter, E. Kapit, R. Thomale, and M. Greiter, *Phys. Rev. Lett.* **99**, 097202 (2007).
- [19] P. A. Lee, *Science* **321**, 1306 (2008).
- [20] S. V. Isakov, M. B. Hastings, R. G. Melko, *Nat. Phys.* **7**, 772 (2011).
- [21] H. Yao and S. A. Kivelson, *Phys. Rev. Lett.* **108**, 247206 (2012).
- [22] F. Wang, *Phys. Rev. B* **82**, 024419 (2010).
- [23] Y. M. Lu and Y. Ran, *Phys. Rev. B* **84**, 024420 (2011).
- [24] B. K. Clark, D. A. Abanin, and S. L. Sondhi, *Phys. Rev. Lett.* **107**, 087204 (2011).
- [25] H. C. Jiang, H. Yao, and L. Balents, *Phys. Rev. B* **86**, 024424 (2012).
- [26] R. Ganesh, J. V. D. Brink, and S. Nishimoto, *Phys. Rev. Lett.* **110**, 127203 (2013).
- [27] Z. Y. Zhu, D. A. Huse, and S. R. White, *Phys. Rev. Lett.* **110**, 127205 (2013).
- [28] S. S. Gong, D. N. Sheng, O. I. Motrunich, and M. P. A. Fisher, *Phys. Rev. B* **88**, 165138 (2013).
- [29] S. S. Gong, W. Zhu, D. N. Sheng, O. I. Motrunich, and M. P. A. Fisher, *Phys. Rev. Lett.* **113**, 027201 (2014).
- [30] H. C. Jiang, Z. Y. Weng, and D. N. Sheng, *Phys. Rev. Lett.* **101**, 117203 (2008).
- [31] S. Yan, D. Huse, and S. R. White, *Science* **332**, 1173 (2011).
- [32] S. Depenbrock, I. P. McCulloch, and U. Schollwöck, *Phys. Rev. Lett.* **109**, 067201 (2012).
- [33] H. C. Jiang, Z. H. Wang, and L. Balents, *Nat. Phys.* **8**, 902 (2012).
- [34] A. Kitaev, J. Preskill, *Phys. Rev. Lett.* **96**, 110404 (2006).
- [35] M. Levin, X. G. Wen, *Phys. Rev. Lett.* **96**, 110405 (2006).
- [36] L. Balents, M. P. A. Fisher, and C. Nayak, *Phys. Rev. B* **60**, 1654 (1999).
- [37] Y. C. He, D. N. Sheng, and Y. Chen, *Phys. Rev. B* **89**, 075110 (2014).
- [38] Y. Ran, M. Hermele, P. A. Lee, and X. G. Wen, *Phys. Rev. Lett.* **98**, 117205 (2007).
- [39] Y. Iqbal, F. Becca, and D. Poilblanc, *Phys. Rev. B* **84**, 020407(R) (2011).
- [40] S. S. Gong, W. Zhu, and D. N. Sheng, *Sci. Rep.* **4**, 6317 (2014).
- [41] Y. C. He, D.N. Sheng, and Y. Chen, *Phys. Rev. Lett.* **112**, 137202 (2014).
- [42] R. B. Laughlin, *Phys. Rev. Lett.* **50**, 1395 (1983).
- [43] V. Kalmeyer and R. B. Laughlin, *Phys. Rev. Lett.* **59**, 2095 (1987).
- [44] X. G. Wen, F. Wilczek, and A. Zee, *Phys. Rev. B* **39**, 11413 (1989).
- [45] K. Yang, L. K. Warman, and S. M. Girvin, *Phys. Rev. Lett.* **70**, 2641 (1993).
- [46] F. D. M. Haldane and D. P. Arovas, *Phys. Rev. B* **52**, 4223 (1995).
- [47] J. W. Mei and X. G. Wen, arXiv:1407.0869.
- [48] Y. C. He and Y. Chen, arXiv:1407.2740.
- [49] B. Bauer, L. Cincio, B. P. Keller, M. Dolfi, G. Vidal, S. Trebst, A. W. W. Ludwig, arXiv:1401.3017.
- [50] M. Barkeshli, arXiv:1307.8194.
- [51] Y. Shimizu, K. Miyagawa, K. Kanoda, M. Maesato, and G. Saito, *Phys. Rev. Lett.* **91**, 107001 (2003).
- [52] Y. Kurosaki, Y. Shimizu, K. Miyagawa, K. Kanoda, and G. Saito, *Phys. Rev. Lett.* **95**, 177001 (2005).
- [53] T. Itou, A. Oyamada, S. Maegawa, M. Tamura, and R. Kato, *Phys. Rev. B* **77**, 104413 (2008).
- [54] P. Mendels, F. Bert, M. A. de Vries, A. Olariu, A. Harrison, F. Duc, J. C. Trombe, J. S. Lord, A. Amato, and C. Baines, *Phys. Rev. Lett.* **98**, 077204 (2007).
- [55] J. S. Helton, K. Matan, M. P. Shores, E. A. Nytko, B. M. Bartlett, Y. Yoshida, Y. Takano, A. Suslov, Y. Qiu, J.-H. Chung, D. G. Nocera, and Y. S. Lee, *Phys. Rev. Lett.* **98**, 107204 (2007).
- [56] M. A. de Vries, J. R. Stewart, P. P. Deen, J. O. Piatek, G. J. Nilsen, H. M. Rønnow, and A. Harrison, *Phys. Rev. Lett.* **103**, 237201 (2009).
- [57] B. Fåk, E. Kermarrec, L. Messio, B. Bernu, C. Lhuillier, F. Bert, P. Mendels, B. Koteswararao, F. Bouquet, J. Ollivier, A. D. Hillier, A. Amato, R. H. Colman, and A. S. Wills, *Phys. Rev. Lett.* **109**, 037208 (2012).
- [58] T. H. Han, J. S. Helton, S. Chu, D. G. Nocera, J. A. Rodriguez-Rivera, C. Broholm, and Y. S. Lee, *Nature* **492**, 7429 (2012).
- [59] L. Clark, J. C. Orain, F. Bert, M. A. De Vries, F. H. Aidoudi, R. E. Morris, P. Lightfoot, J. S. Lord, M. T. F. Telling, P. Bonville, J. P. Attfield, P. Mendels, and A. Harrison, *Phys. Rev. Lett.* **110**, 207208 (2013).
- [60] I. A. McDonald and F. D. M. Haldane, *Phys. Rev. B* **53**, 15845 (1996).
- [61] X. G. Wen, *Phys. Rev. Lett.* **84**, 3950 (2000).
- [62] S. R. White, *Phys. Rev. Lett.* **69**, 2863 (1992).
- [63] See more information in Supplemental Material.
- [64] L. Cincio and G. Vidal, *Phys. Rev. Lett.* **110**, 067208 (2013).
- [65] Michael P. Zaletel, Roger S. K. Mong, and Frank Pollmann, *Phys. Rev. Lett.* **110**, 236801 (2013).
- [66] P. Di Francesco, P. Mathieu, and D. Senechal, *Conformal Field Theory* (Springer, New York, 1997), Chap. 15.6.
- [67] H. Li and F. D. M. Haldane, *Phys. Rev. Lett.* **101**, 010504 (2008).
- [68] Y. Hatsugai, *Phys. Rev. Lett.* **71**, 3697 (1993).
- [69] W. Zhu, S. S. Gong, and D. N. Sheng, *J. Stat. Mech.* 2014 (8), P08012.
- [70] A. G. Grushin, J. Motruk, M. P. Zaletel, and F. Pollmann, arXiv:1407.6985.
- [71] X. L. Qi, H. Katsura, A. W. W. Ludwig, *Phys. Rev. Lett.* **108**, 196402 (2012).
- [72] While one cannot get a few low energy singlet excitations in DMRG accurately, one can obtain the triplet gap E_T by targeting the ground states in the different total S^z sectors separately.
- [73] C. Waldtmann, H. U. Everts, B. Bernu, C. Lhuillier, P. Sindzinger

gre, P. Lecheminant, L. Pierre, Eur. Phys. J. B **2**, 501 (1998).

SUPPLEMENTAL MATERIAL

INFINITE DMRG ALGORITHM

We also use the infinite density matrix renormalization group (iDMRG) [1] to study this model. In the iDMRG algorithm, we first start from a small system size. Then we insert one column in the center and optimize the energy by sweeping the inserted column. After the optimization, we absorb the new column into the original existing system and get the new boundary Hamiltonians. We repeat the inserting, optimizing and absorbing procedure until the energy convergence is achieved. Compared with the finite DMRG simulation, iDMRG grows the lattice by one column at each iteration and only sweeps the inserted column, thus the computation cost is significantly reduced. iDMRG is especially efficient to deal with the gapped topological order system, which allows us to obtain the ground states with well-defined anyonic flux as first proposed in Ref. [2]. In our work, we have confirmed that the iDMRG obtains the fixed-point ground state wavefunction in the center of cylinder that is exactly the same as that obtained from the finite DMRG simulations (the same energy and the identical entanglement spectrum within the numerical error.).

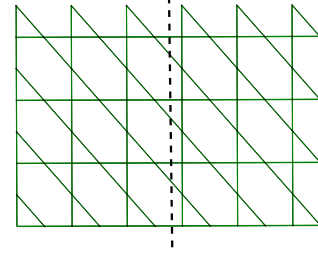
ENTANGLEMENT SPECTRUM ON XC GEOMETRY

There are two kinds of cylinder geometry on kagome lattice often being studied in DMRG, YC-geometry in SFig. 5(a) and XC-geometry in SFig. 5(b). In the main text, the demonstrated results are all based on YC-geometry. Here we show that the entanglement spectrum and the spectrum flow shown on YC-geometry are robust and insensitive to the lattice geometry. In SFig. 6, we demonstrate the entanglement spectrum flow for $J_z = 0, J'_{xy} = 0.1$ on $L_y = 6$ XC-geometry. The features of the spectrum flow are consistent with the results on YC-geometry shown in Fig. 3(a) of the main text. The eigenvalues in $S^z = 1$ and $S^z = -1$ sectors are degenerate at $\theta = 0$. By increasing flux θ , the eigenvalues in $S^z = 1$ sector flow up while those in $S^z = -1$ sector flow down continuously. At $\theta = 2\pi$, the eigenvalues in the $S^z = 0$ and $S^z = -1$ sectors become degenerate, which results in a fractionally quantized Chern number $C = 1/2$. Thus, the phase diagram shown in the main text is robust for different geometries.

CHIRAL VELOCITY FROM ENTANGLEMENT SPECTRUM

Entanglement spectrum resembles the edge excitation spectrum that can be viewed as a fingerprint of topological order. In the main text, we show the entanglement spectrum at $J_z = 0.0, J'_{xy} = 0.3$ in Figs. 1(c) and 1(d). The characteristic chiral edge spectrum indicates the chiral spin liquid (CSL) state. Here we show the spectrum at $J_z = 0.0, J'_{xy} = 0.1$ on

(a) YC-geometry



(b) XC-geometry

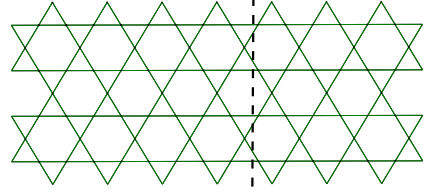


FIG. 5: (color online) Kagome cylinder on (a) YC geometry and (b) XC geometry. The cylinders are closed in the y direction and opened in the x direction.

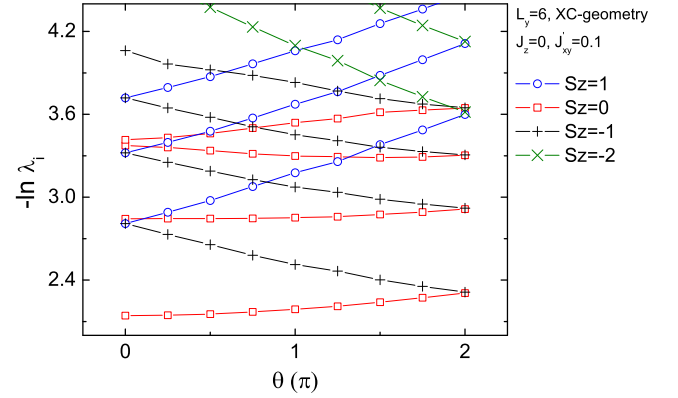


FIG. 6: (color online) Entanglement spectrum flow for $J_z = 0.0, J'_{xy} = 0.1$ on $L_y = 6$ XC cylinder, which is obtained by keeping 3000 states.

YC-geometry, which is closer to the phase boundary $J'_{xy} \simeq 0.06J_{xy}$. As shown in SFig. 7, the entanglement spectrum also exhibits the degeneracy pattern $\{1, 1, 2, 3, 5, \dots\}$ consistent with the CSL state.

Entanglement spectrum gives not only the characteristic degeneracy pattern of the edge excitation, but also the edge-mode velocity [3]. In the conformal field theory, the edge-mode of the Laughlin state is described by a single branch of chiral charged bosons. The velocity of the charged bosons v_c is not an universal quantity as it depends on the microscopic interaction and edge confinement. In the cylinder geometry, we can define v_c through the lowest values of entanglement spectrum with edge momentum $k = 0$ and $k =$

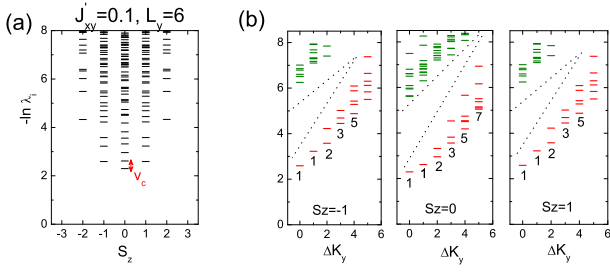


FIG. 7: (color online) (a) Entanglement spectrum for $J_z = 0.0$, $J'_{xy} = 0.1$ on $L_y = 6$ YC cylinder, which is obtained by keeping 3000 states. The red arrow denoted as v_c indicates the two lowest values in $k = 0$ and $2\pi/L_y$ sectors that are used to calculate the chiral velocity. (b) Near degenerating pattern for the low-lying entanglement spectra with different relative momentum Δk_y and total spin S^z for the same system in (a). Δk_y is in unit of $2\pi/6$.

$\frac{2\pi}{L_y}$: $v_c = \frac{\Delta E}{\hbar \Delta k} = \frac{E_0(k=2\pi/L_y) - E_0(k=0)}{\hbar 2\pi/L_y}$, where $E_0(k) = \min\{-\ln \lambda(k)\}$ is the lowest eigenvalue with edge momentum k . Thus, from our results on YC-geometry, we have

$\frac{v_c(J'_{xy}=0.1)}{v_c(J'_{xy}=0.3)} \approx 0.439$. Although the CSL state is still robust at $J'_{xy} = 0.1$, the edge-mode velocity is reduced compared to $J'_{xy} = 0.3$ in the deep CSL phase. With further decreasing J'_{xy} , we find that the difference of the lowest value between the momentum sectors $k = 0$ and $k = 2\pi/L_y$ continuously decreases before the quantum phase transition takes place. The reducing of chiral velocity obtained from entanglement spectrum is related with the drop of the bulk excitation gap with decreasing J'_{xy} , which is consistent with a very weakly first order transition or a continuous transition driven by the collapsing of the bulk gap and the destruction of the gapless edge states at the same time.

-
- [1] I. P. McCulloch, arXiv:0804.2509.
 - [2] L. Cincio and G. Vidal, Phys. Rev. Lett. **110**, 067208 (2013).
 - [3] Z. X. Hu, E. H. Rezayi, X. Wan, and K. Yang, Phys. Rev. B **80**, 235330 (2009).